A honeycomb multilevel structure Bi_2O_3 with highly efficient catalytic activity driven by bias voltage and oxygen defect

Tong Chen[a1], Qiang Hao[a1], Wenjuan Yang[b, c], Chenlang Xie[a], Daimei Chen[a]*, ChaoMa[b], Wenqing Yao[b]* and Yongfa Zhu[b]*

a Beijing Key Laboratory of Materials Utilization of Nonmetallic Minerals and Solid Wastes, National Laboratory of Mineral Materials, School of Materials Science and Technology, China University of Geosciences, Beijing 100083, China

b Department of Chemistry, Tsinghua University, Beijing, 100084, PR China)

c School of Chemistry and Chemical Engineering, Yulin University, Yulin City 719000, Shaanxi, China.

1: These authors contributed the same to this manuscript

*Corresponding author.

Tel.: +86 15801558907; fax: +86 10 82322974.

E-mail: chendaimei@cugb.edu.cn;

E-mail: yaowq@tsinghua.edu.cn; zhuyf@tsinghua.edu.cn

Abstract

In this work, we report a bismuth oxide film electrode with oxygen defects and honeycomb multilevel structure prepared by one-step hydrothermal method. The control of raw materials enables to control the thickness and morphology of Bi_2O_3 electrodes. The photoelectrocatalytic activity of prepared electrodes was tested in various conditions. Under visible light irradiation ($\lambda \geq 420$ nm) and 3 V bias, the sample BiO–2 has the highest photoelectrocatalytic activity, which is 4.95 times higher than the photocatalytic activity and 9.86 times higher than the electrocatalytic activity. The oxygen defects of bismuth oxide were confirmed by EPR. The morphology and structure of prepared samples were tested by XRD, scanning electronic microscope (SEM), high-resolution transmission electron microscope (HRTEM) and X-ray photoelectron spectroscopy (XPS). The enhanced photoelectrocatalytic activity is attributed to the proper bias voltage, oxygen defects, and honeycomb multilevel structure. The results of trapping experiments showed that the main active species during the photoelectrocatalytic progress was superoxide radical and hydroxyl radical. Finally, the mechanism of the photoelectrocatalysis was proposed.

1. Introduction

In recent years, the large-scale production and consumption of antibiotics has become a serious problem, and the abuse of antibiotics is widespread [1-3]. The residue of antibiotics in water environment has attracted the wide attention of researcher [4, 5]. The long-standing presence of antibiotics and their decomposition products enables to lead to drug-resistant bacteria [6, 7]. What's worse, the antibiotic resistance genes can transfer and spread extremely fast, which seriously affects the ecological system. Therefore, it is urgent to find a low-cost and efficient treatment method for antibiotic wastewater [8]. Common treatment methods of antibiotic wastewater include precipitation [9], extraction [10, 11], biological treatment and photocatalytic degradation [12-21]. The precipitation and extraction cannot completely degrade the

pollutant in wastewater, but only adsorb and enrich the waste. Biological treatment, at present, is a highly efficient way. However, the cost of this progress is quite high and it is difficult for it to be applied. Compared with these methods, photocatalytic technology has broad potential in the field of wastewater control because it is environmentally friendly, low-cost and highly efficient [22]. However, the photocatalytic degradation efficiency is not up to the requirements of practical applications. This is mainly due to the rapid recombination of photogenerated charge carriers and low utilization of solar energy [23]. More importantly, it is difficult to separate and recycle the powder catalysts from the water [24].

Therefore, scientists hope to use the synergistic effect to improve the efficiency of photocatalytic materials. Thus, a lot of synergistic effects of materials have been developed, such as photoelectrocatalysis and microwave-photo-assisted catalytic materials [25-28]. Even some researchers use the synergistic effect of adsorption and photodegradation to improve catalytic activity [29]. Among them, photoelectric catalysis has received extensive attention for it has a lot of advantages such as simple synthetic method, low energy consumption and high efficiency [30-33]. A lot of ultraviolet-light response photoelectric catalysts have been developed in the past several years [30, 31]. Nevertheless, ultraviolet light accounts for merely 4% of solar energy [34]. Although the performance of conventional photocatalyst (ZnO, TiO_2) is efficient, the utilization of solar energy is still not ideal. As a result, scientists pay more attention to visible light responsive photocatalysts [17].

Liang et al. reported a facile preparation of C_3N_4 film electrode on indium–tin oxide (ITO) glass, which exhibited excellent photoelectrocatalytic activity [27]. Zhao et al. plated Bi_2MoO_6 on the surface of boron-doped diamond (BDD) glass and used it for photoelectrocatalytic degradation of ibuprofen and naproxen [35]. The results showed that ibuprofen and naproxen could be degraded by photoelectrocatalysis under visible light irradiation and the degradation and mineralization rate were both higher than that of the sum of photocatalysis and electrocatalytic oxidation. However, there

are still some barriers to the application of photoelectrocatalytic materials. With ITO, FTO, BDD, SnO_2 as the basal electrode, the cost is quite high and the powder on the basal electrode always easily peel off, leading to a drop in photoelectrocatalytic activity [27, 30, 31, 35].

Bismuth oxide (Bi_2O_3) is one of the simplest bismuth-based semiconductor photocatalysts [17, 36, 37]. Recently, researchers paid a lot of attention to Bi_2O_3 because of its facile preparation, low cost, unique electronic structure, low valence band position, narrow band gap and excellent visible light response ability [38, 39]. Bi_2O_3 is often prepared by heating $Bi(NO_3)_3$ at a high temperature (more than 600 °C) and it has four kinds of crystalline form，including α, β, γ and δ form, which are monoclinic crystalline form, tetragonal crystalline form, body-centered cubic crystalline form and face-centered cubic crystalline form, respectively [40, 41]. Compared with other Bi_2O_3, δ–Bi_2O_3 is fluorite structure and it has the highest oxygen ion conductivity among all compounds [42]. More importantly, it has a lot of oxygen defects, which is helpful for photocatalytic activity [42, 43].

However, δ–Bi_2O_3 is a high-temperature stable phase (710–824 °C) and it is difficult to prepare δ–Bi_2O_3 under a relatively mild condition. In addition, photogenerated electron-hole pairs recombine fast, and the photo quantum efficiency of δ–Bi_2O_3 is not high. Therefore, the photocatalytic activity of bismuth oxide is limited. Photoelectrocatalysis has a broad prospect of overcoming these difficulties [44, 45].

In this work, a multilevel structure δ–Bi_2O_3 electrode with oxygen defects was prepared by a facile one-step hydrothermal method in a relatively mild condition. Titanium sheet was used as a basal electrode, and the quantity of raw materials enabled to control the thickness and structure of Bi_2O_3. When the Bi_2O_3 film coating was 2.70 μm, and the bias voltage was 3 V, the sample has the best photoelectrocatalytic performance, which was 4.95 times higher than the photocatalytic activity and 9.86 times higher than the electrocatalytic activity. The method has the advantages of simple preparation, low cost and excellent catalytic effect. At the same time, the reaction

mechanism of photoelectrocatalytic degradation of Bi_2O_3 was proposed, which has great significance of fundamental research and application of photoelectric catalysis.

2. Experimental Section

The bismuth nitrate was brought from Sinopharm Chemical Reagent Beijing Co., Ltd. The sodium sulphate was brought from Tianjin Guangfu Fine Chemical Research Institute. The glycol, ethanol and acetone were brought from Beijing Chemical Works. The tetracycline was brought from Beijing Solarbio Technology Co., Ltd. All chemicals used were of reagent grade and used without further purification.

2.1. Preparation of Electrode

24 mL of glycol was added to 48 mL of acetone in a beaker. 0.48 g of $Bi(NO_3)_3 \cdot 5H_2O$ was weighed and added into the solution. After stirring for an hour, the solution was transferred into a Teflon kettle whose capacity is 100 mL. A titanium sheet (50 mm * 25 mm) was added as substrate. The solution was heated at 160 °C for 6 h. After cooling to room temperature, titanium sheet with Bi_2O_3 were taken out and soaked in pure water for half an hour to remove residual organic impurities and it was dried at 60 °C for 6 h. This sample was named as BiO–1. When only $Bi(NO_3)_3 \cdot 5H_2O$ dosage was changed, the sample prepared with 0.96 g $Bi(NO_3)_3 \cdot 5H_2O$ was named as BiO–2, and the sample prepared with 1.44 g $Bi(NO_3)_3 \cdot 5H_2O$ was named as BiO–3.

2.2. Characterization and Catalytic Activity

The morphology and structure of as-prepared samples were characterized by scanning electron microscopy (SEM; HITACHI SU-8010) at 10 kV and 10 μA and high resolution transmission electron microscopy (HRTEM; JEOL2100F) at 100 kV. The component of as-prepared samples was investigated by X-ray diffraction (XRD; D/max-2400) at 25 °C. X-ray photoelectron spectroscopy (XPS) of as-prepared samples

was conducted on a PHI Quantera XPS. UV-vis diffuse reflection spectra (DRS) were obtained from a HITACHI U-3900 UV-vis spectrometer, using $BaSO_4$ as reference. Photoluminescence spectra were tested by fluorescence spectrometer (HITACHI F-4600) at 25 °C. The electron paramagnetic resonance spectra were determined by using the electron paramagnetic resonance (EPR; JES-FA200) technique at 123 K.

The i-t current and electrochemical impedance spectroscopy (EIS) was performed from a CHI-760 E (China) electrochemical workstation with a standard three-electrode cell, including counter electrode (Pt wire), reference electrode (saturated calomel electrode) and working electrodes (as-prepared film electrodes). 0.1 M sodium sulfate solution was used as electrolyte solution, and a 100 mL square quartz tank was employed as the reaction tank. The electrochemical impedance spectra (EIS) were obtained in the frequency range of 0.01–100000 Hz with an amplitude of 5 mV. The cyclic voltammetry scans and stability of electrode were obtained in the potential range of 0.5–2 V, at the same time, its scan rate was 0.1 V/s and the solution was Na_2SO_4 (0.1 mol/L) and tetracycline (10 ppm). The Mott-Schottky curves were acquired in the voltage range of -2–2 V with a scanning speed of 0.1 V/s and a scanning frequency of 1000 Hz. When testing the Mott-Schottky curves, the counter electrode was a Pt wire and the reference electrode was an Ag/AgCl electrode. Degradation of the tetracycline was performed on a high performance liquid chromatography (HPLC) system (Shimadzu LC-20AT). In the first six minutes，the compositions of mobile phase was oxalic acid (0.005 M, pH= 2.4), acetonitrile and methanol (71:16:13, V/V/V). After 6 minutes, the composition of the mobile phase was converted to oxalic acid (0.005 M, pH = 2.4), acetonitrile and methanol (50:25:25, V/V/V). After fifteen minutes, it returned to its original composition. The mobile phase flow rate was 1 mL/min and the determined wavelength was 360 nm. Elution time was within 11 minutes. Chromatographic separations were operated by using Venusil XBP-C18 column (3.9 × 200, Agela Technologies Inc).

Tetracycline was used as a molecular probe with an initial concentration of 10 ppm. The light source was supplied by a 300 W xenon lamp (CEL-PF300-T8, Beijing China Education Au-light Co., Ltd) with a cutoff filter (420 nm). The distance between the

light and the working electrode was 20.0 cm, and the photoelectrocatalytic degradation process lasted for five hours. 3 mL solution was sampled per hour, and the concentration of the solution was recorded by the absorbance of tetracycline at 375 nm. The experimental method for electrocatalysis and photocatalysis are the same as those above without the addition of light or voltage.

2.3. Trapping Experiment

Based on the experiment of photoelectric catalysis, 1 mmol tert-butanol, 1 mmol KI and 1mmol para-benzoquinone were added into the tetracycline solution and they are the inhibitors of hydroxyl radicals, holes and superoxide radicals, respectively. Other operations are identical to the test of photoelectrocatalytic performance.

2.4. DFT Calculation

The ionic positions of the starting structures were optimized by the projector augmented wave (PAW) method with the Perdew-Burke-Ernzerhof (PBE) exchange correlation functional in the Vienna ab initio simulation package (VASP, version 5.3.2) [46]. Throughout the calculations, the convergence criterion of the total energy was set to 10^{-5} eV and Hellmann–Feynman force was smaller than 0.02 eV $Å^{-1}$ in the self-consistent field. The cutoff energy for the plane-wave basis set was set to 400 eV. The atoms were relaxed and reoptimized with a conjugate gradient (CG) method. The numerical integration in the first Brillouin zone is performed using a Monkhorst–Pack grid of 7 × 7 × 7.

3. Results and Discussion

3.1. Photoelectric degradation performance

XRD is one of the most common research methods for studying the composition of materials, the structure of atoms and the information about molecules or crystals inside the materials [47, 48]. As shown in **Fig. S**1, the peaks of the three samples can be indexed to δ–Bi_2O_3 (01-078-5636) without impurity peaks. **Fig. 1**a is the optical

photograph of the prepared Bi_2O_3 electrode and it can be seen that the Bi_2O_3 powder film grew uniformly on basal titanium sheet. The photoelectrocatalytic activity of samples is evaluated by the degradation of tetracycline. To investigate the effects of different voltages on photoelectrocatalytic activity, the photoelectrocatalytic activity of BiO–2 under various voltages is tested. As shown in **Fig. 1**b, when the voltage is 0.5 V or 1 V, the catalytic activity is quite weak. When the voltage improves to 2 V, the catalytic effect improves evidently. When the voltage is 3 V, the catalytic activity reaches the maximum, and when it enhances to 4 V, the catalytic efficiency reduces a lot. Among them, the rate constant of 3 V is 0.253, which is 4.14 times higher than that of 1 V and it is 2.45 times higher than that of 4 V. After that, the photoelectrochemical degradation efficiency of different samples under visible light irradiation and 3 V is investigated. **Fig. 1**c is the apparent rate constant for photoelectrocatalytic degradation efficiency of tetracycline under visible light irradiation ($\lambda > 420$ nm) and the voltage is 3 V. It can be seen that the degradation efficiency of BiO-2 is the highest. It can be informed that BiO–2 had the highest degradation efficiency, which is 1.93 times higher than that of BiO–1 and 3.40 times higher than that of BiO–3. Combined with **Fig. 1**b and c, it can be inferred that when the bias voltage is 3 V and the sample is BiO-2, the photocatalytic degradation is the highest. To further confirm the effect of the Bi_2O_3 electrode, a contrast experiment was employed, and the result is shown in **Fig. 1**d. When visible light or bias voltage is applied separately, BiO–2 shows quite low catalytic activity. Nevertheless, the synergistic of photo and electric catalysis can greatly enhance the degradation efficiency. The photoelectrocatalytic activity of the BiO–2 is 4.95 times higher than that of photocatalysis and it is 9.86 times higher than that of electrocatalytic oxidation. As for pure titanium sheet, it has few catalytic activity under visible light irradiation or bias voltage. The synergistic of photo and electric catalysis enable to improve the catalytic activity of titanium sheet, but there is still a huge gap between it and BiO–2 electrode. From **Fig. 1**d, it can be concluded that the synergistic of photo and electric catalysis enable to enhance the catalytic of the Bi_2O_3 electrode greatly. The results of degradation dynamics and HPLC are provided in **Fig. S**2 and **S**3. From these results, the degradation of tetracycline can be further confirmed.

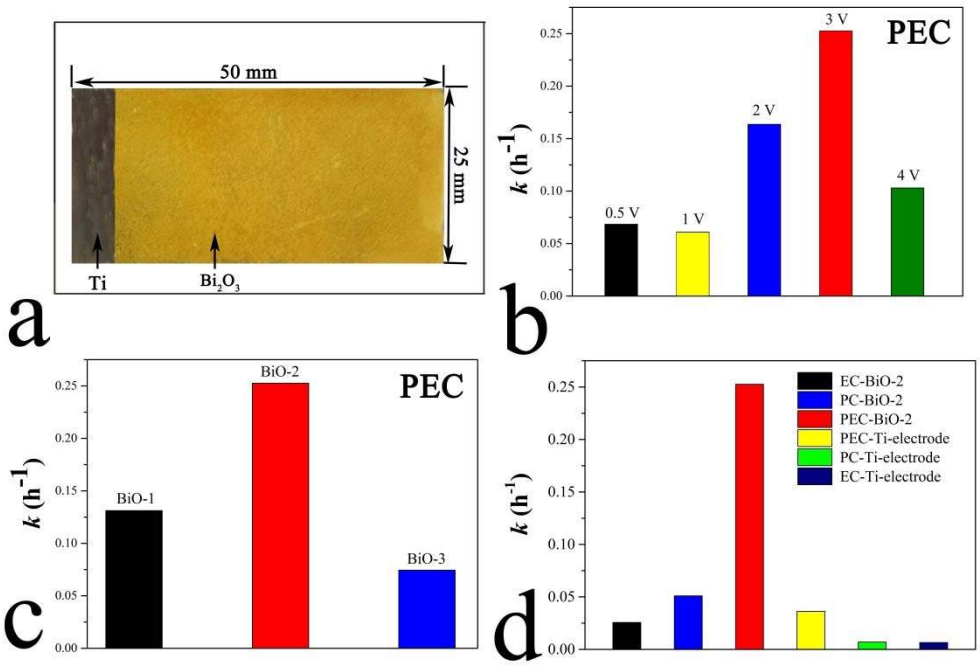

Fig. 1. (a) Optical photograph of the prepared film electrodes. (b) The comparison of the PEC degradation apparent rate constant *k* of tetracycline over Bi_2O_3 film electrode at various potentials. (c) The photoelectrocatalysis efficiency of different samples under visible light irradiation and 3 V voltage. (d) Apparent rate constants for tetracycline degradation over BiO–2 film electrode and pure titanium sheet under various conditions.

Fig. 2 is the cyclic voltammetry scans of the sample BiO–2 in a 0.1 M Na_2SO_4 solution with 10 ppm tetracycline. It can be seen that the oxidation peak of tetracycline appeared at nearly 1.2 V [49]. When the voltage is less than 1.2 V, it does not have electrocatalytic effect on the oxidation of tetracycline. When the bias voltage improves to 1.2 V, tetracycline began to be degraded rapidly and when the bias voltage increases to 1.5 V, water molecules on the electrode surface are oxidized and decomposed, producing some strong oxidizing substance, such as hydroxyl radical, superoxide radical or oxygen [50, 51]. Thus, the degradation rate of tetracycline is enhanced. When the voltage reaches 3 V, the catalytic activity is the strongest. However, when the voltage is greater than 3 V, the oxidation of tetracycline intermediates on the surface of the electrode forming a thin film， which seriously hindered the reaction, resulting in a decrease in the reaction rate [27, 52].

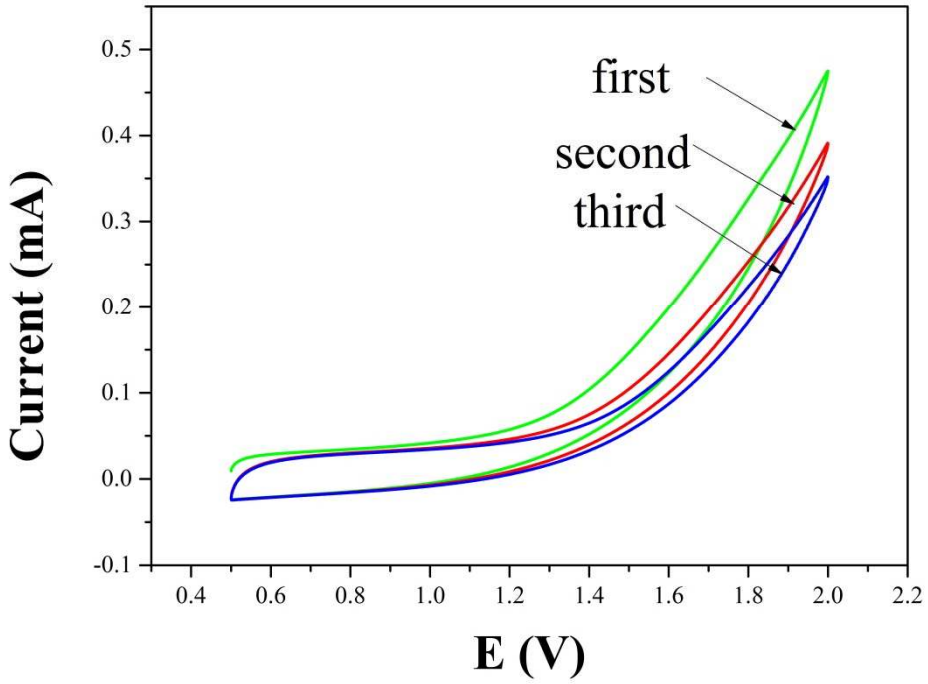

Fig. 2. Cyclic voltammetry scans with the BiO–2 film electrode in a 0.1 M Na_2SO_4 electrolyte with 10 ppm tetracycline.

3.2. Structure and morphology

The morphology and size of the Bi_2O_3 photocatalyst are observed by scanning electron microscopy (SEM) [53]. It can be obtained from the results of SEM-EDX mapping images that the samples consist of Bi and O elements (**Fig. S4**). **Fig. 3**a and b are SEM images of BiO–1. It shows a uniform microspheres structure, and the diameter is about 0.21 μm. **Fig. 3**c and d are the SEM images of BiO–2, which are obviously different from figure 3a. It can be seen that the sample BiO–2 is a globular structure, while the size is different. In general, there are two kinds of microspheres, the diameter of the bigger one is about 2.7 μm and the other is 0.21μm. As shown in **Fig. 3**d, the BiO–2 is a multilevel structure that is assembled into three-dimensional globular structures by two-dimensional nanosheet. There are also some small microspheres, the diameter of which is the same as that of BiO–1. **Fig. 3**e and f are the SEM images of BiO–3. They are also multilevel globular structure, but the diameters of the spheres increased a lot. The large microspheres have a diameter of 3.3 μm and the content of

smaller microspheres reduced. Compared with BiO–2, an obvious reunion occurs and the size of microspheres increases, which are caused by the increasing use of raw materials. SEM was employed to test the thickness of Bi_2O_3 film on the surface of Ti sheet. As shown in **Fig. S5**, the thickness of BiO–1, BiO–2 and BiO–3 are 11.9 μm, 61.6 μm and 71.9 μm, respectively.

More detailed information on the microstructure of Bi_2O_3 samples is further investigated by HRTEM [54]. In **Fig. 4**b, the lattice spacing of 0.306 nm and 0.314 nm is corresponding to the (400) and (222) plane of δ–Bi_2O_3, respectively. Through the EDS-Mapping, it can be confirmed that the sample is composed of two elements, Bi and O.

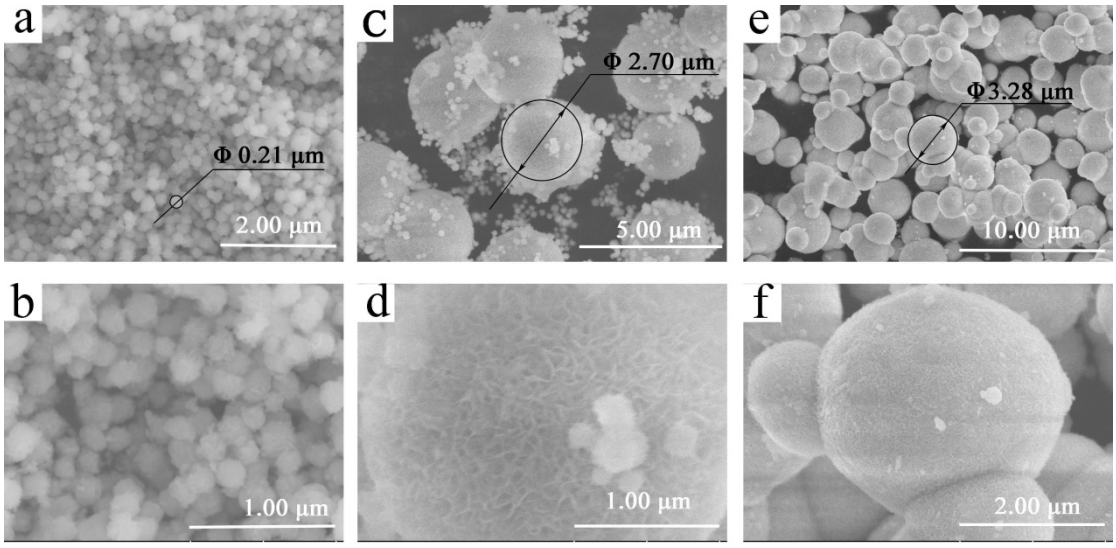

Fig. 3. (a-b) SEM images of sample BiO–1. (c-d) SEM images of sample BiO–2. (e-f) SEM images of sample BiO–3.

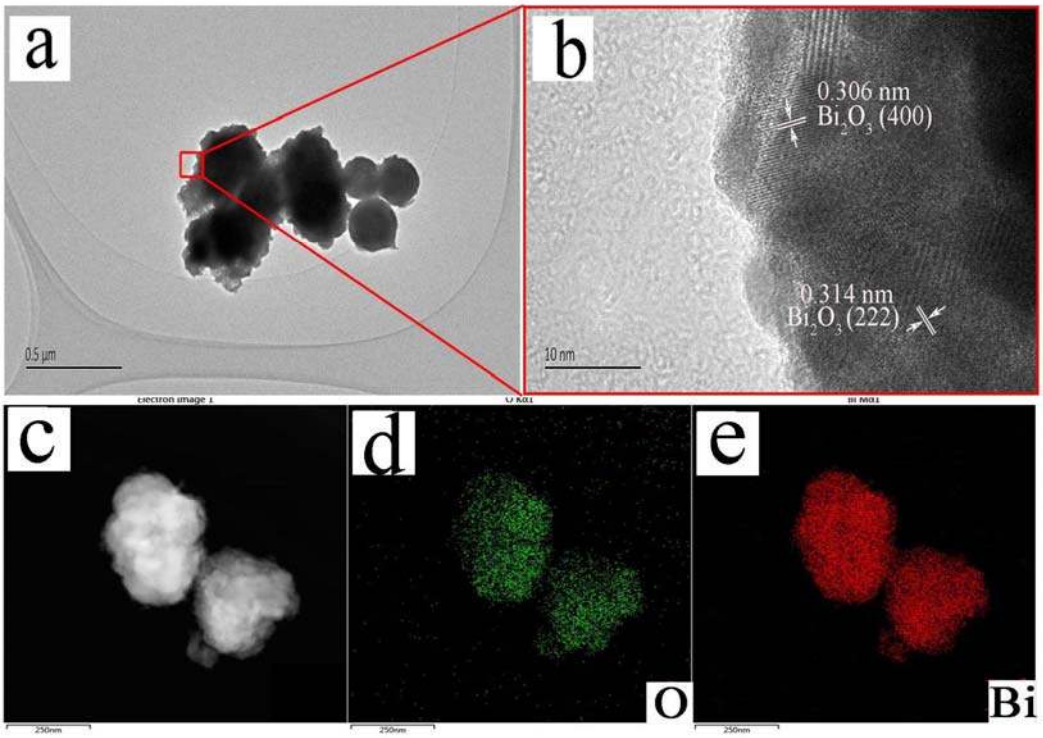

Fig. 4. (a-b) HRTEM images of sample BiO–2. (c-e) TEM-EDX (mapping) of BiO–2 (c), (d) and (e).

3.3. Reaction Mechanism

3.3.1. Band gap of materials

UV-vis diffuse reflectance spectrum (DRS) is employed to study the optical properties of materials. It can be seen that the samples have a broad absorption in the visible light region [55]. With the increasing use of bismuth nitrate ($BiNO_3$), the absorption edge of prepared samples shows a redshift and it shifts from 3.13 to 2.79 eV, which is caused by the increasing particle size and the quantum size effect of nanomaterials. To further study the band structure of prepared Bi_2O_3 samples，the Mott-Schottky curves are tested and shown in **Fig. S**6. According to the Mott-Schottky curves and UV–vis DRS, the band structure of Bi_2O_3 samples is obtained (**Fig. 6**). The VB of BiO–2 is 2.64 eV and it is the most positive in the three samples, which means that it has the strongest oxidation ability.

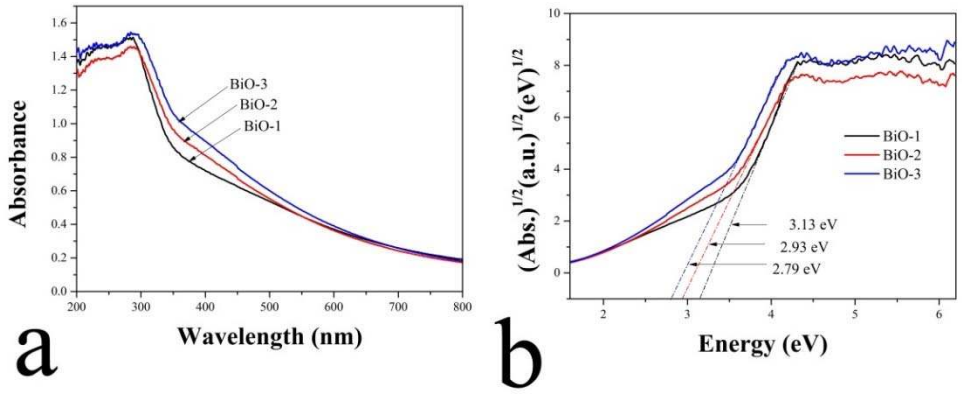

Fig. 5. (a) UV–vis diffuse reflectance spectra (DRS) and (b) band gaps of prepared samples.

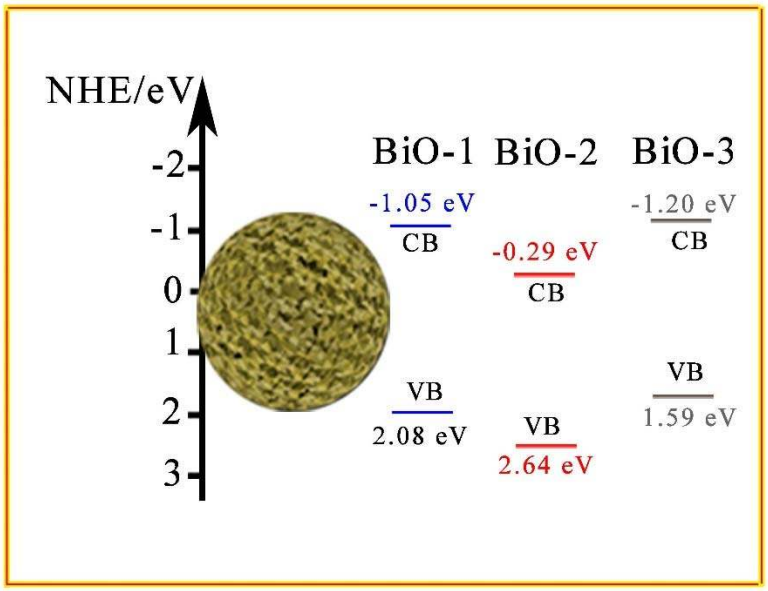

Fig. 6. The band structure of prepared Bi_2O_3 samples.

3.3.2. Oxygen defects and photoelectric properties

XPS is always employed to study the chemical composition of materials [34]. **Fig. 7**a is the survey XPS spectrum of prepared samples, indicating that they consist of O and Bi element. **Fig. 7**b is the narrow spectrum of oxygen elements. As it can be seen, the peaks of BiO–2 obviously shift to higher binding energy, which is probably caused by oxygen defects. To further verify the existence of oxygen defects, the electron paramagnetic resonance (EPR) of BiO–2 is tested. As shown in **Fig. 7**c, BiO–2 has the strongest oxygen defect signal, indicating it has more oxygen defects. Therefore, due to the large quantity of oxygen defects, the BiO–2 sample has the highest

photoelectrochemical catalytic activity. Photocurrent and EIS are used to investigate the separation efficiency of photogenerated electron-hole pairs [17]. As shown in **Fig. 7**d, all the prepared Bi_2O_3 electrodes rapidly produce a stable photocurrent response when visible light is irradiated. BiO–2 has the strongest light responsive current, indicating that more photogenerated carriers are produced. BiO–2 has the lowest arc radius in the EIS Nyquist plot in **Fig. 7**e, which means that the separation of photogenerated charge carriers was most effective. This should also be a very important reason why BiO–2 has the highest photoelectrocatalytic performance. In order to further investigate the separation and recombination of photoinduced charge carriers, fluorescent spectra of prepared samples are tested. The fluorescent spectra intensity of BiO–2 is the lowest, indicating that BiO–2 has a relatively low rate of recombination of photogenerated electrons, which is helpful for the transfer and separation of photoinduced electron-hole pairs [56].

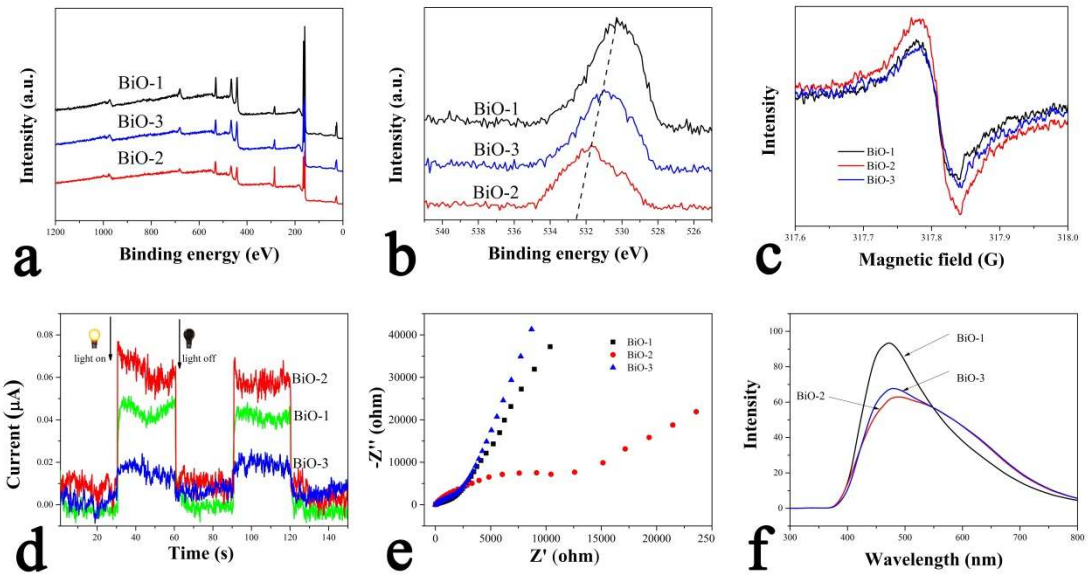

Fig. 7. XPS spectra of the sample BiO–1, BiO–2 and BiO–3: (a) survey spectrum; (b) O 1*s* spectrum. (c) EPR of sample BiO–1, BiO–2 and BiO–3. (d) The transient photocurrent responses of sample BiO–2 electrodes with light on/off cycles under visible light irradiation (λ > 420 nm). (e) Electrochemical impedance spectroscopy (EIS) of prepared samples under visible light irradiation (λ>420nm). (f) Photoluminescence spectra of prepared samples.

3.3.3. Trapping experiment

To investigate the respective effect of photoactive radical on the degradation of tetracycline, trapping experiments are performed using different radical scavengers, which is helpful to understand the mechanism of the photoelectric catalytic reaction. P-benzoquinone (BQ) is the scavenger of superoxide radicals, tert-butanol is the scavenger of hydroxyl radicals and KI is the scavenger of holes [46]. The corresponding experimental results are listed as follow [17]. When BQ is added, the removal efficiency is less than 10%, while KI has no obvious influence on the photoelectrocatalytic performance of the sample. When tert-butanol is added, the photoelectrocatalytic activity is also decreased, and it means that hydroxyl radicals also played an important role in the photoelectrocatalytic progress. Clearly, this indicates that superoxide radicals and hydroxyl radicals are the main reactive species of Bi_2O_3 in the photoelectric catalytic reaction.

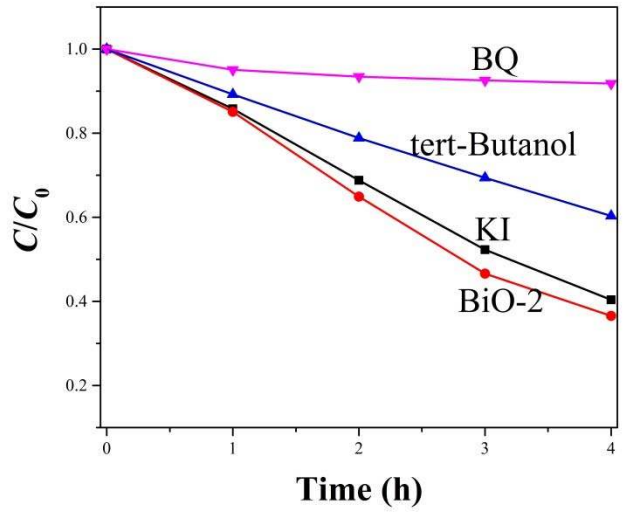

Fig. 8. Effects of different trapping agents on the photocatalytic activity of BiO–2 film electrode.

3.3.4. Calculation result

The density states of pure δ–Bi_2O_3 show that it has a band gap of 2.63 eV with O 2*p* and Bi 3*s* as valence band maximum. The calculated value of band gap is smaller than that of experimental data owing to the underestimate of DFT to describe excited states. The band gap of defect δ–Bi_2O_3 is about 1.00 eV with some hybrid bands mainly consists of oxygen 2*p* orbitals. We can find the band gap of defect δ–Bi_2O_3 is smaller

than that of pure δ–Bi_2O_3, indicating that it can absorb more visible light and it can be excited more easily.

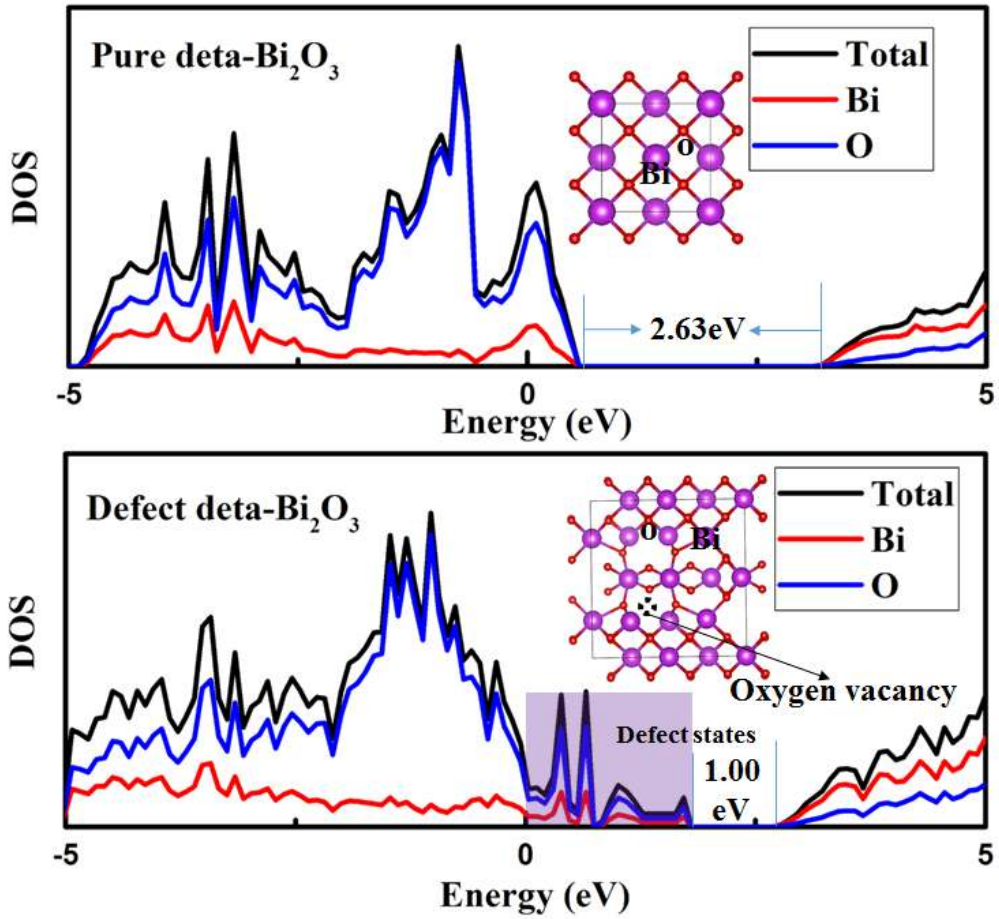

Fig. 9. Density states of pure δ–Bi_2O_3 and defect δ–Bi_2O_3 with its atomic structure, purple area indicates defect states coming from the oxygen vacancy.

3.3.5 Stability of electrode

The stability of BiO–2 electrode was tested by CV for 1000 cycles. As shown in **Fig. S7**, the current gradually decreased in the 1000 cycles, indicating that the stability of BiO–2 electrode was not very good. This is because δ–Bi_2O_3 is a high-temperature stable phase and the fluorite-type structure is not stable.

Based on the above experimental results, a possible mechanism is proposed. As shown in **Scheme. 1**, under visible light irradiation, the semiconductor is excited, and electron-hole pairs are produced. Electrons can react with oxygen to produce superoxide radicals. The hole itself has the capability of direct oxidation, and it can also

react with water to generate hydroxyl radicals. They are all highly reactive species with strong oxidizing activity. Thus, the tetracycline can be degraded. In general, the recombination rate of electrons and holes is very fast and most of them cannot participate in the catalytic reaction. In photoelectrocatalysis progress, the transfer and separation of the photoinduced charges enable to be accelerated by the external bias voltage. As a result, the recombination rate of the electron-hole pair is greatly decreased and the degradative efficiency can be highly improved. Photocatalysis and electrocatalysis play a synergistic catalytic role with each other. Generally, electrocatalysis can be divided into two types: direct catalysis and indirect catalysis. When the voltage is below 1.2 V, direct oxidation occurs to form an intermediate film, which covers the sample electrode and inhibits further degradation of tetracycline and the presence of intermediates on the electrode can be prevented by visible light irradiation. When the voltage is higher than 1.5 V, indirect oxidation occurs. Water molecules at the surface of the Bi_2O_3 film electrode can be discharged and generate O_2. Under visible light irradiation, O_2 as electronic acceptor, produce more superoxide radical, which can participate in the oxidation of tetracycline and intermediates. Therefore, degradation of tetracycline can be maximized at a suitable voltage. However, when the voltage is over 3 V, the system generates a large number of O_2, which can react with hydroxyl radicals leading to the decrease of hydroxyl radicals, so that the intermediate product is not further degraded and forming a film covering the electrode [52, 57]. The reaction is further hindered and the rate of degradation begins to decrease. More importantly, BiO-2 had more oxygen defects than the other samples, which can narrow the bandgap, make the VB of Bi_2O_3 more positive and work as trapping sites of oxygen molecules. The defects and honeycomb multilevel structure made it easier for oxygen to be absorbed on the surface of the electrode and react with electrons. As a result, more superoxide radicals are generated.

At the same time, the proper bias could also improve the photocatalytic activity. With the introduction of an electrical field, the photogenerated electrons trended to transfer to the Pt electrode, as a result, the separation efficiency of photogenerated electron-hole pairs was greatly improved.

The photoelectrocatalytic performance of sample BiO–2 is optimum, which can be considered in the following aspects: first of all, the film electrode has a suitable thickness, which is 61.6 μm. When the thickness of the electrode is thinner, less active species are produced. When the thickness of the sample is too thicker, the particles agglomerate and the separation of photogenerated carriers are hindered, resulting in the recombination of the electron-hole pairs. Secondly, the sample BiO–2 has more oxygen defects which can adsorb pollutants and help to generate more active species. Finally, the BiO–2 sample has a honeycombed spherical structure composed of lamellae with a larger surface area that facilitates the attachment and reaction of pollutants.

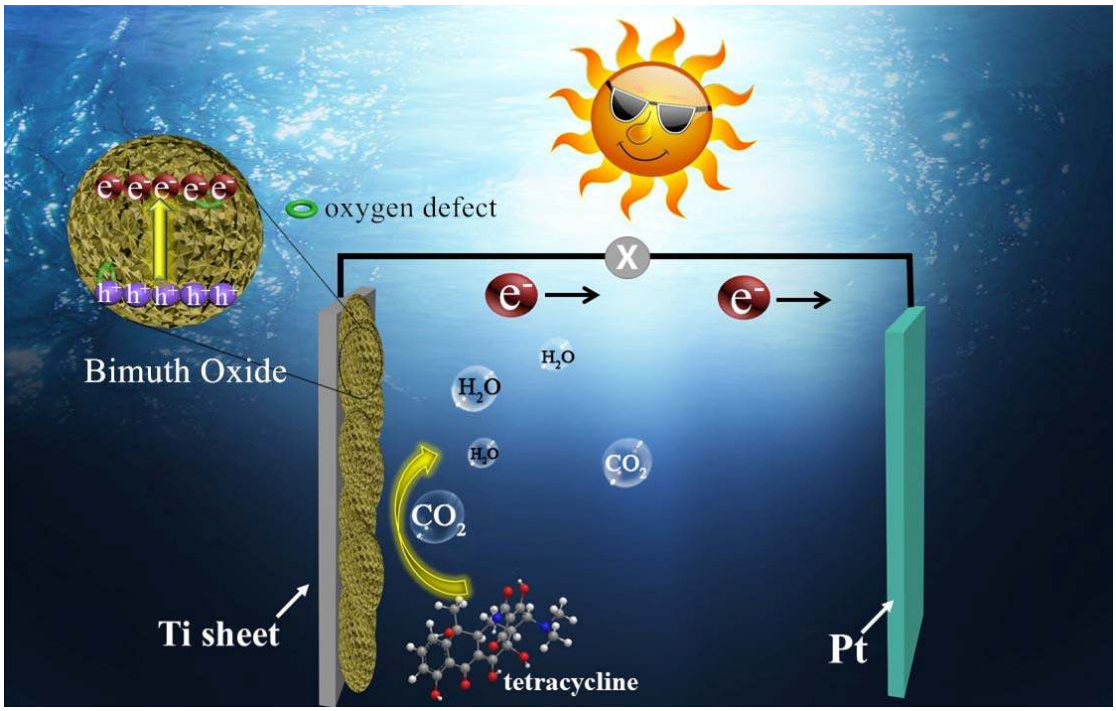

Scheme.1 Mechanism for the photodegradation of tetracycline of Bi_2O_3 driven by bias voltage and oxygen defect

4. Conclusions

In this work, a bismuth oxide film electrode with oxygen defects and honeycomb multilevel structure is prepared by one-step hydrothermal method. Under visible light irradiation ($\lambda \geq 420$ nm) and 3 V bias, the sample BiO–2 has the highest photoelectrocatalytic activity, which is 4.95 times higher than the photocatalytic activity and 9.86 times higher than the electrocatalytic activity. The enhanced

photoelectrocatalytic activity is attributed to the proper bias voltage, the large quantity of oxygen defects and honeycomb multilevel structure. The bias voltage enables to decompose water molecules and produce oxygen, which is able to react with electrons and produce more superoxide radicals. Oxygen defects and honeycomb multilevel structure provided more trapping sites for oxygen and pollutant. As a result, more active species are generated and the degradation efficiency is enhanced.

Acknowledgements

This work is supported by the National Natural Science Foundation of China (Grant No. 21577132, 21777080, 51651201), the Fundamental Research Funds for the Central Universities (Grant No. 2652015225), the Students Innovation and Entrepreneurship Training Program 2017 (2017AB026) of China University of Geosciences Beijing. Tsinghua National Laboratory for Information Science and Technology and Collaborative Innovation Center for Regional Environmental Quality. Our work is completed on the “Explorer 100” cluster system of Tsinghua National Laboratory for Information Science and Technology.

Reference

[1] H. Su, S. Liu, X. Hu, X. Xu, W. Xu, Y. Xu, Z. Li, G. Wen, Y. Liu, Y. Cao, Sci. Total Environ. 607 (2017) 357-366.
[2] M. Bourdat-Deschamps, S. Ferhi, N. Bernet, F. Feder, O. Crouzet, D. Patureau, D. Montenach, G.D. Moussard, V. Mercier, P. Benoit, S. Houot, Sci. Total Environ. 607 (2017) 271-280.
[3] E. Bloem, A. Albihn, J. Elving, L. Hermann, L. Lehmann, M. Sarvi, T. Schaaf, J. Schick, E. Turtol, K. Ylivainio, Sci. Total Environ. 607 (2017) 225-242.
[4] F. Baquero, J.-L. Martinez, R. Canton, Curr. Opin. Biotech. 19 (2008) 260-265.
[5] M.-T. Guo, G.-S. Zhang, Chemosphere 183 (2017) 197-203.
[6] J. Hrenovic, G. Durn, M.S. Music, S. Dekic, T. Troskot-Corbic, D. Skoric, Sci. Total Environ. 607 (2017) 1049-1055.

[7] C. Vuotto, F. Longo, C. Pascolini, G. Donelli, M.P. Balice, M.F. Libori, V. Tiracchia, A. Salvia, P.E. Varaldo, J. Appl. Microbiol. 123 (2017) 1003-1018.
[8] C. Adams, Y. Wang, K. Loftin, M. Meyer, J. Eviron. Eng. 128 (2002) 253-260.
[9] S. Golbaz, A.J. Jafari, M. Rafiee, R.R. Kalantary, Chem. Eng. J. 253 (2014) 251-257.
[10] M. Cizmic, S. Babic, M. Kastelan-Macan, Environ. Sci. Pollut. R. 24 (2017) 20521-20539.
[11] W. Kujawski, A. Warszawski, W. Ratajczak, T. Porebski, W. Capala, I. Ostrowska, Desalination 163 (2004) 287-296.
[12] Y.-L. Lin, J. Membrane Sci. 542 (2017) 342-351.
[13] H. Temmink, K. Grolle, Bioresource Technol. 96 (2005) 1683-1689.
[14] H.H.P. Fang, D.W. Liang, T. Zhang, Y. Liu, Water Res. 40 (2006) 427-434.
[15] F. Chen, Q. Yang, F. Yao, S. Wang, J. Sun, H. An, K. Yi, Y. Wang, Y. Zhou, L. Wang, X. Li, D. Wang, G. Zeng, J. Catal. 352 (2017) 160-170.
[16] X.-J. Wen, C.-G. Niu, M. Ruan, L. Zhang, G.-M. Zeng, J. Colloid Interf. Sci. 497 (2017) 368-377.
[17] Q. Hao, R. Wang, H. Lu, C.a. Xie, W. Ao, D. Chen, C. Ma, W. Yao, Y. Zhu, Appl. Catal. B 219 (2017) 63-72.
[18] Q. Hao, X. Niu, C. Nie, S. Hao, W. Zou, J. Ge, D. Chen, W. Yao, Phys. Chem. Chem. Phys. 18 (2016) 31410-31418.
[19] Y. Guo, X. Lou, D. Xiao, L. Xu, Z. Wang, J. Liu, J. Hazard. Mater. 241 (2012) 301-306.
[20] R. Yuan, S.N. Ramjaun, Z. Wang, J. Liu, Chem. Eng. J. 192 (2012) 171-178.
[21] J. Fu, J. Yu, C. Jiang, B. Cheng, Adv. Energy Mater. (2017) 1701503.
[22] S. Han, L. Hu, Z. Liang, S. Wageh, A.A. Al-Ghamdi, Y. Chen, X. Fang, Adv. Funct. Mater. 24 (2014) 5719-5727.
[23] C. Sotelo-Vazquez, R. Quesada-Cabrera, M. Ling, D.O. Scanlon, A. Kafizas, P.K. Thakur, T.-L. Lee, A. Taylor, G.W. Watson, R.G. Palgrave, J.R. Durrant, C.S. Blackman, I.P. Parkin, Adv. Funct. Mater. 27 (2017) 1605413.
[24] P. Fakhri, B. Jaleh, M. Nasrollahzadeh, J. Mol. Catal. A 383 (2014) 17-22.
[25] X. Wang, G. Wang, S. Chen, X. Fan, X. Quan, H. Yu, J. Membrane Sci. 541 (2017) 153-161.
[26] Q. Zeng, J. Li, L. Li, J. Bai, L. Xia, B. Zhou, Appl. Catal. B 217 (2017) 21-29.
[27] F. Liang, Y. Zhu, Appl. Catal. B 180 (2016) 324-329.
[28] Y. Ju, S. Yang, Y. Ding, C. Sun, A. Zhang, L. Wang, J. Phys. Chem. A 112 (2008) 11172-11177.
[29] N.X.D. Mai, J. Bae, I.T. Kim, S.H. Park, G.-W. Lee, J.H. Kim, D. Lee, H. Bin Son, Y.-C. Lee, J. Hur, Environ. Sci.: Nano 4 (2017) 955-966.
[30] S. Song, Y. Zhang, Y. Xing, C. Wang, J. Feng, W. Shi, G. Zheng, H. Zhang, Adv. Funct. Mater. 18 (2008) 2328-2334.
[31] K. Vinodgopal, I. Bedja, P.V. Kamat, Chem. Mater. 8 (1996) 2180-2187.
[32] Y. Wang, J. Lin, R. Zong, J. He, Y. Zhu, J. Mol. Catal. A 349 (2011) 13-19.
[33] J. Lin, R. Zong, M. Zhou, Y. Zhu, Appl. Catal. B 89 (2009) 425-431.
[34] L. Ge, F. Zuo, J. Liu, Q. Ma, C. Wang, D. Sun, L. Bartels, P. Feng, J. Phys. Chem. C 116 (2012) 13708-13714.
[35] X. Zhao, J. Qu, H. Liu, Z. Qiang, R. Liu, C. Hu, Appl. Catal. B 91 (2009) 539-545.
[36] C. Yu, K. Wang, P. Yang, S. Yang, C. Lu, Y. Song, S. Dong, J. Sun, J. Sun, Appl. Surf. Sci. 420 (2017) 233-242.
[37] Y. Bao, T.-T. Lim, Z. Zhong, R. Wang, X. Hu, J. Colloid Interf. Sci. 505 (2017) 489-499.

[38] C. Diaz-Guerra, P. Almodovar, M. Camacho-Lopez, S. Camacho-Lopez, J. Piqueras, J. Alloy. Compd. 723 (2017) 520-526.
[39] N. Yavo, A.D. Smith, O. Yeheskel, S.R. Cohen, R. Korobko, E. Wachtel, P.R. Slater, I. Lubomirsky, Adv. Funct. Mater. 26 (2016) 1138-1142.
[40] A. Hameed, T. Montini, V. Gombac, P. Fornasiero, J. Am. Chem. Soc. 130 (2008) 9658-9759.
[41] Z. Bian, J. Zhu, S. Wang, Y. Cao, X. Qian, H. Li, J. Phys. Chem. C 112 (2008) 6258-6262.
[42] M. Tsubaki, K. Koto, Mater. Res. Bull. 19 (1984) 1613-1620.
[43] D.S. Aidhy, S.B. Sinnott, E.D. Wachsman, S.R. Phillpot, J.C. Nino, J. Solid State Chem. 182 (2009) 1222-1228.
[44] X. Zhao, H. Liu, J. Qu, Appl. Surf. Sci. 257 (2011) 4621-4624.
[45] C. Li, J. Zhang, K. Liu, Int. J. Electrochem. Sci. 7 (2012) 5028-5034.
[46] R. Palominos, J. Freer, M.A. Mondaca, H.D. Mansilla, J. Photoch. Photobio. A 193 (2008) 139-145.
[47] B. Chen, X. He, F. Yin, H. Wang, D.-J. Liu, R. Shi, J. Chen, H. Yin, Adv. Funct. Mater. 27 (2017) 1700795.
[48] K. Kaliyappan, J. Liu, B. Xiao, A. Lushington, R. Li, T.-K. Sham, X. Sun, Adv. Funct. Mater. 27 (2017) 1701870.
[49] H.J. Yang, A.J. Bard, J. Electroanal. Chem. 339 (1992) 423-449.
[50] G.W. Muna, N. Tasheva, G.M. Swain, Environ. Sci. Technol. 38 (2004) 3674-3682.
[51] O. Simond, V. Schaller, C. Comninellis, Electrochim. Acta. 42 (1997) 2009-2012.
[52]R. Pelegrini, J. Reyes, N. Duran, P.P. Zamora, A.R. de Andrade, J. Appl. Electrochem. 30 (2000) 953-958.
[53] Q. Hao, S. Hao, X. Niu, X. Li, D. Chen, H. Ding, Chinese J. Catal. 38 (2017) 278-286.
[54] Z. Weng, H. AminiRastabi, Z. Xiong, H. Xue, J. Alloy Compd. 725 (2017) 1063-1068.
[55] J. Zhang, Z. Liu, Z. Liu, ACS Appl. Mater. Inter. 8 (2016) 9684-9691.
[56] M.R. E-Ghobashy, A.M. Yehia, A.H. Helmy, N.F. Youssef, Spectrochim. Acta. A 188 (2018) 619-625.
[57] X. Zhao, Y.F. Zhu, Environ. Sci. Technol. 40 (2006) 3367-3372.